nanoenergy advances

MDPI

Article

Preparation and Characterization of Amide-Containing Polyimide Films with Enhanced Tribopositivity for Triboelectric Nanogenerators to Harvest Energy at Elevated Temperatures

Zhen Pan [1], Shunqi Yuan [2], Yan Zhang [1], Xi Ren [1], Zhibin He [3], Zhenzhong Wang [1], Shujun Han [1], Yuexin Qi [1], Haifeng Yu [3] and Jingang Liu [1,*]

[1] Engineering Research Center of Ministry of Education for Geological Carbon Storage and Low Carbon Utilization of Resources, School of Materials Science and Technology, China University of Geosciences, Beijing 100083, China; 2103210036@email.cugb.edu.cn (Z.P.); 3003200016@email.cugb.edu.cn (Y.Z.); renxi@email.cugb.edu.cn (X.R.); wzz0808@163.com (Z.W.); 15966200097@163.com (S.H.); qiyuexin1004@163.com (Y.Q.)

[2] RAYITEK Hi-Tech Film Company, Co., Ltd., Shenzhen 518105, China; sq.yuan@rayitek.cn

[3] Key Laboratory of Polymer Chemistry and Physics of Ministry of Education, School of Material Science and Engineering, Peking University, Beijing 100871, China; zb.he@stu.pku.edu.cn (Z.H.); yuhaifeng@pku.edu.cn (H.Y.)

* Correspondence: liujg@cugb.edu.cn; Tel.: +86-10-8232-2972

Abstract: As triboelectric nanogenerator (TENG) technology continue to evolve, its application in harsh environments has increasingly captivated the interest of researchers. However, the current research on heat-resistant triboelectric materials remains predominantly focused on the development of tribo-negative materials, with scant attention given to their equally crucial tribo-positive counterparts. In this study, the tribo-positive polyimide (PI) material with enhanced tribo-positivity is developed by integrating amide groups with electron-donating effects into the molecular chain. Furthermore, the TENG devices based on this series of tribo-positive PI materials have demonstrated an open-circuit voltage (V_{OC}) of 242 V, a short-circuit current (I_{SC}) of 8.13 μA, and a transferred charge (Q_{SC}) of 117 nC. Notably, these devices also demonstrate the capability to efficiently generate electricity even under elevated temperature conditions. This work not only proposes a potential molecular design strategy for developing high-performance tribo-positive PI materials applicable in TENGs, but also markedly propels the advancement of robust energy-harvesting devices engineered for operation at elevated temperatures.

Keywords: triboelectric nanogenerators; polyimide; amide; thermal properties; high temperature

Citation: Pan, Z.; Yuan, S.; Zhang, Y.; Ren, X.; He, Z.; Wang, Z.; Han, S.; Qi, Y.; Yu, H.; Liu, J. Preparation and Characterization of Amide-Containing Polyimide Films with Enhanced Tribopositivity for Triboelectric Nanogenerators to Harvest Energy at Elevated Temperatures. *Nanoenergy Adv.* **2024**, *4*, 284–299. https://doi.org/10.3390/nanoenergyadv4030017

Academic Editors: Renyun Zhang and Sangmin Lee

Received: 8 July 2024
Revised: 29 August 2024
Accepted: 6 September 2024
Published: 12 September 2024

1. Introduction

Triboelectric nanogenerators (TENGs) represent a groundbreaking advancement in energy-harvesting technology, ingeniously combining the principles of contact electrification and electrostatic induction to efficiently convert mechanical energy into electrical energy. Distinguished from other energy-harvesting technologies, TENGs excel in capturing low-frequency, irregular energy sources [1–7]. Meanwhile, TENGs are becoming forefront technologies in the arena of new energy devices, attributed to their scalability, versatile design, and a broad range of material choices. With ongoing research and an expanding array of applications, the suitability of these generators for demanding environments characterized by extreme temperatures and humidity is garnering increasing recognition [8–12]. Nevertheless, this broadening introduces new challenges in terms of material selection and the stability of equipment performance.

Extensive research has been dedicated to the selection and preparation of materials to facilitate the broader application of triboelectric nanogenerators (TENGs), ensuring their reliability and performance in harsh environments [13–16]. For instance, Qian et al.

innovatively employed poly(*p*-phenylenebenzobisoxazole) (PBOA) aerogels in the negative friction layer of TENGs, achieving effective energy harvesting and conversion at high temperatures. The high porosity and substantial specific surface area of PBOA aerogels enabled TENGs to attain a maximum open-circuit voltage of 40 V, a short-circuit current density of 2.9 mA/m^2, and a charge density of 72 $\mu C/m^2$. Impressively, these TENGs were capable of charging a capacitor to 10 V in just 250 s and efficiently powering several small light bulbs [17]. Additionally, polyimide (PI) materials have attracted considerable attention in the triboelectric field for excellent properties, including outstanding triboelectric characteristics and superior charge storage capacity. The molecular structure of PI, which contains numerous imide and various functional groups, offers abundant charge-trapping sites and excellent electron-withdrawing abilities. These features facilitate effective charge trapping, rendering PI materials ideal for creating high-efficiency friction layers [18–21]. Furthermore, the exceptional mechanical properties ensure durability and stability through repeated use, while their superior heat resistance broadens the operational temperature range, significantly enhancing the application potential of PI materials [22–26]. For instance, the work conducted by Tao et al. achieved a remarkable enhancement in the triboelectric properties and thermal-charge stability of PI by incorporating potent electron-absorbing groups into its main chain and doping it with $BaTiO_3$ nanoparticles. These modifications tightened the LUMO (lowest unoccupied molecular orbital) energy band distributions, thereby improving charge-trapping capabilities. Furthermore, the introduction of $BaTiO_3$ nanoparticles created additional electron traps and interfacial polarization effects, which further augmented the charge-trapping and storage capacity, culminating in a substantial increase in charge density. The TENG based on this composite PI film maintained a 32% effective output at a high temperature of 200 °C in a hot air tunnel, showcasing considerable application potential [27].

Moreover, Xing et al. made a notable advancement in TENG technology by integrating silica aerogel into the PI electrospinning process, resulting in the development of multilayer triboelectric yarns. In performance tests, the TENG, which utilized the PI nanocomposite layer as applied material, demonstrated a remarkable transferred charge density of 30 nC/cm^2 and a peak power output of 0.17 mW. Crucially, this device demonstrated the capability to harvest electrical energy and detect biological motion across a wide temperature range of 25 to 400 °C, thereby substantially extending the operational threshold of electronic devices [28]. Despite these advancements, the majority of research has predominantly focused on the development of tribo-negative materials. In contrast, the exploration of tribo-positive materials, which are equally crucial for enhancing surface charge density and facilitating efficient charge transfer, has been comparatively neglected, thus hindering the application of TENG devices in harsh conditions. On the other hand, Li et al. took a different approach by irradiating conventional commercial Kapton® films that widely applied negative friction layer with low-energy helium (He) ions. The experiments revealed that He ion irradiation effectively altered the surface functional groups of the Kapton® film, converting tribo-negative imide groups into tribo-positive amide groups. The alteration in chemical structure not only realized the triboelectric conversion of the Kapton® film, but also endowed it with superb electron-donating capabilities and excellent charge stability, unveiling a significant advancement and a novel tribo-positive material option for TENG technology [29]. Consequently, the diversity in the molecular structure of PI polymers and the correlation with triboelectric properties have prompted further research into modifying molecular structures to develop tribo-positive PI materials suitable for high-temperature environments.

In the present study, the chemical bonding and functional groups of the PI triboelectric polymers were adjusted at the molecular level to develop a novel tribo-positive amide-containing PI material. Furthermore, calculation methods like density functional theory (DFT) were employed to elucidate the relationship between the molecular structure and triboelectric properties from the perspective of changes in molecular orbital energy levels, with a view to inspire the design of triboelectric materials. Based on the

above, an all-PI-based TENG was constructed by integrating fluorinated PI composite film assemblies. This design culminates in an effective electrical energy output in high-temperature environments.

2. Materials and Methods

2.1. Materials

The aromatic dianhydride 4,4′-(4,4′-isopropylidenediphenoxy)bis(phthalic anhydride) (BPADA) with a purity exceeding 99.5% was purchased from Beijing Innochem Science & Technology Co., Ltd. (Beijing, China), then being subjected to vacuum drying at 180 °C for 24 h prior to use. The amide-containing diamines, including 4,4′-diaminobenzoylanilide (DABA, purity: 99.6%), 2,3′-dimethyl-4,4′-diaminobenzoylanilide (MMDABA, purity: 99.6%), 2-methyl-4,4′-diaminobenzoylanilide (MeDABA, purity: 99.6%), and 2-chloro-4,4′-diaminobenzoylanilide (ClDABA, purity: 99.6%) were supplied by Hitachi Chemical Company., Ltd. (Tokyo, Japan). Polyamide 6 (PA6) was sourced from Zig Sheng Industrial Co., Ltd. (Taiwan, China) and used directly. Formic acid was obtained from Shanghai Macklin Biochemical Technology Co., Ltd. (Shanghai, China). Other tribo-negative materials including Polytetrafluoroethylene (PTFE) film (thickness: 30 μm) and Polydimethylsiloxane (PDMS) film (thickness: 50 μm) were purchased from Sigma Aldrich, Shanghai, China, Sigma-Aldrich (Shanghai, China) Trading Co., Ltd. (Shanghai, China), and were used without further modification. Furthermore, PVDF (polyvinylidene difluoride) powder was obtained from Arkema (China) Investment Co., Ltd. (Paris, France). Electronic-grade *N*,*N*-dimethylacetamide (DMAc, purity: 99.9%, water content < 50 ppm) was also sourced from Beijing Innochem Science & Technology Co., Ltd. (Beijing, China).

2.2. Characterization Methods

To investigate the physical and chemical characteristics of PI films, several analytical techniques were employed. Fourier transform infrared (FTIR) spectra were captured using a Shimadzu Iraffinity-1S FT-IR spectrometer (Kyoto, Japan), encompassing a wavenumber range from 4500 cm^{-1} to 400 cm^{-1}. The Rigaku D/max-2500 X-ray diffractometer (Tokyo, Japan) facilitated the wide-angle X-ray diffraction (XRD) analysis. Differential scanning calorimetry (DSC) was performed using a TA-Q100 system (New Castle, DE, USA) under a nitrogen atmosphere, with a heating rate of 10 °C/min. The thermal decomposition temperature of PI films was determined via a PerkinElmer STA-8000 thermogravimetric analyzer (Perkin-Elmer, Waltham, MA, USA) in a nitrogen environment at a heating rate of 20 °C/min, spanning from 30 to 750 °C. For thermo-mechanical analysis (TMA), a TMA402F3 system (NETZSCH, Selb, Germany) was conducted in a nitrogen atmosphere with a heating rate of 5 °C/min, spanning temperatures from 50 to 450 °C, to ascertain the coefficients of linear thermal expansion (CTE) of the films within the 50 to 200 °C range. Ultraviolet-visible (UV-Vis) spectra of the PI films were captured at room temperature using a Hitachi U-3210 spectrophotometer (Tokyo, Japan). The color parameters of the PI films were assessed employing the CIE Lab equation, where L* denotes lightness on a scale ranging from 0 (black) to 100 (white). The X-rite color i7 spectrophotometer (Grand Rapids, MI, USA) was utilized to quantify the a* values, with positive values indicating red hues and negative values suggesting green hues.

The electrical properties of the TENGs, including open-circuit voltage (V_{OC}), short-circuit current (I_{SC}), and transferred charge (Q_{SC}), were measured employing a 6517B electrometer (Keithley Instruments, Inc., Cleveland, OH, USA). Kelvin Probe Force Microscopy (KPFM) measurements were performed using the KPFM mode in an atomic force microscopy (AFM) system (Billerica, MA, USA) with a Pt-coated Si probe. The measurements were carried out at an oscillation amplitude of 3 V and a resonance frequency of 1.48 Hz. The geometry of the PI models underwent optimization using Gauss density functional theory (DFT), and the calculations for frontier molecular orbitals provided insights into the electrostatic potentials, the highest occupied molecular orbital (HOMO) energies, the lowest unoccupied molecular orbital (LUMO) energies, and the energy gap

(εHOMO−εLUMO). The simulations and calculations were performed with the Gaussian 09 software, employing the B3LYP exchange-correlation function and a 6−31G(d) basis set.

2.3. Preparation of PI Films

The synthesis of aromatic PI commenced with the selection of the dianhydride monomer BPADA and various diamine monomers containing the electron-donating amide group. Employing the thermal imidation method, a series of novel PI polymers with distinct structures, including PI-a (BPADA-DABA), PI-b (BPADA-MeDABA), PI-c (BPADA-ClDABA), and PI-d (BPADA-MMDABA), were successfully synthesized. The specific synthetic route is illustrated in Figure 1a.

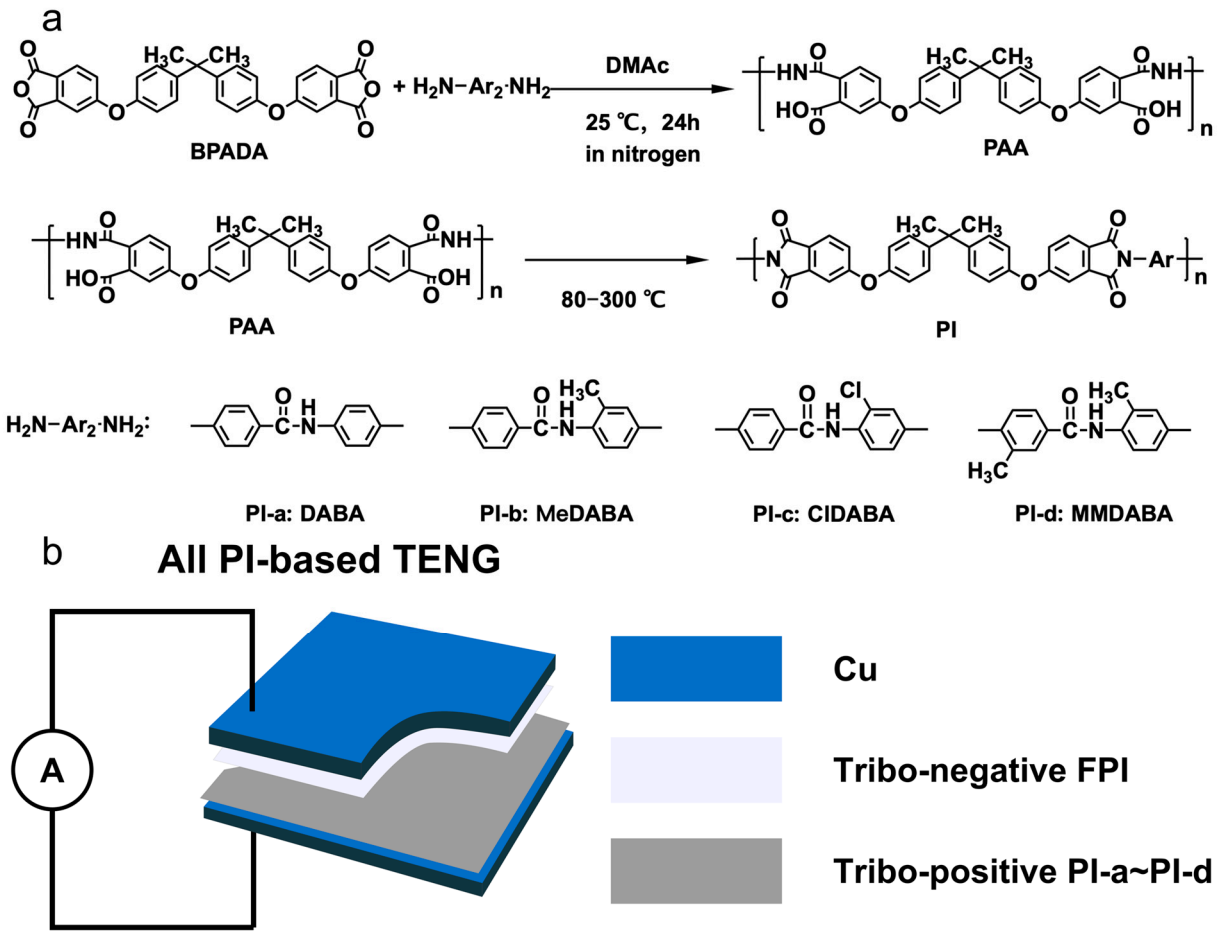

Figure 1. (**a**) Synthesis pathway for PI films, (**b**) the diagram of all PI-based TENGs.

The detailed synthesis procedure could be illustrated by the synthesis of PI-a (BPADA-DABA). Initially, DMAC (149.6 g) and diamine monomer DABA (11.3631 g, 0.05 mol) were added to a 500 mL three-necked flask and stirred under a nitrogen atmosphere until a clear solution formed. Subsequently, the pre-measured dianhydride monomer BPADA (26.0243 g, 0.05 mol) was introduced into the reaction mixture, with additional DMAc being used to rinse any remaining reactants from the flask's interior. Table 1 provides the complete formulation details. After stirring for 24 h at room temperature, the mixture thickened into a high-viscosity poly(amic acid) (PAA) solution. This solution was then evenly cast onto a clean glass plate and subjected to a systematic heat treatment under a nitrogen atmosphere. The temperature increments included 80 °C/h, 120 °C/h, 150 °C/h, 180 °C/h, 200 °C/h, 250 °C/h, and 300 °C/h. Following the heat treatment, the glass plates

with the attached films were cooled and submerged in deionized water, resulting in the production of uniform, flat PI films approximately 30 μm thick.

Table 1. Formula for the PI synthesis.

PI	BPADA (g, mol)	DABA (g, mol)	MeDABA (g, mol)	ClDABA (g, mol)	MMDABA (g, mol)	DMAC (g)
PI-a	26.0243, 0.05	11.3631, 0.05	NA [a]	NA [a]	NA [a]	149.6
PI-b	26.0243, 0.05	NA [a]	12.0631, 0.05	NA [a]	NA [a]	152.3
PI-c	26.0243, 0.05	NA [a]	NA [a]	14.8130, 0.05	NA [a]	163.4
PI-d	26.0243, 0.05	NA [a]	NA [a]	NA [a]	12.7630, 0.05	154.8

[a] Not applicable.

The preparation of other modified amide-containing PI films, including PI-b (BPADA-MeDABA), PI-c (BPADA-ClDABA), and PI-d (BPADA-MMDABA), followed a similar procedure as previously described. However, in these preparations, DABA was replaced with MeDABA for PI-b, with ClDABA for PI-c, and with MMDABA for PI-d.

2.4. Fabrication of TENG Devices

The construction of all TENGs adhered to the traditional vertical contact-separation mode, as depicted in Figure 1b. The assembly process involved the utilization of copper conductive tape, approximately 40 μm thick, for the formation of electrodes. Notably, the tribo-positive layers were innovatively fabricated using PI film (thick: ~30 μm), which had an active contact area of approximately 16 cm^2 (40 mm × 40 mm). Additionally, the preparation of PA6 materials entailed dissolving 10 g of PA6 particles in a 40 g formic acid solution, with continuous magnetic stirring at 40 °C for 5 h to ensure complete dissolution. The resultant PA6 solution was then cast onto a clean glass plate. Following film formation, the film was submerged in deionized water to facilitate phase transition. The film was subsequently peeled off, thoroughly washed to eliminate solvent residues, and dried in an oven at 80 °C for 6 h, yielding the PA6 porous film. For the tribo-negative layer, an FPI composite film with enhanced triboelectric properties was selected, prepared from fluorinated polyimide composite organic semiconductor 1,4,5,8-Naphthalenetetracarboxylic dianhydride (NTCDA) [30]. Furthermore, the integration of the polyethylene terephthalate (PET) film improved the structural integrity of the entire TENG device and greatly increased its durability.

3. Results

3.1. Structural Characterization

The FTIR spectra of the PI films are presented in Figure 2a, exhibiting a sequence of characteristic peaks, indicative of the PI structure within the 450–4000 cm^{-1} wavenumber range. Notably, two prominent absorption peaks at 1780 cm^{-1} and 1720 cm^{-1} correspond to the symmetric and asymmetric stretch vibrations of the imide ring's carbonyl group (C=O), respectively. Additionally, a peak near 1370 cm^{-1} aligns with the C–N bond stretch vibration on the imide ring, confirming the successful formation of the imide ring in the polymer. Furthermore, the interval at 2970 cm^{-1} contains distinctive peaks corresponding to the $–CH_3$ group's stretch vibration within the dianhydride monomer BPADA and the diamine monomer, further substantiating the successful synthesis of the target PI polymer. The aggregated state structures of PI with varying configurations were meticulously characterized, with the findings illustrated in Figure 2b. The analysis indicates that the combined effects of ether bonds and methyl substituents result in a more relaxed configuration of the PI, leading to the manifestation of typical amorphous structural characteristics.

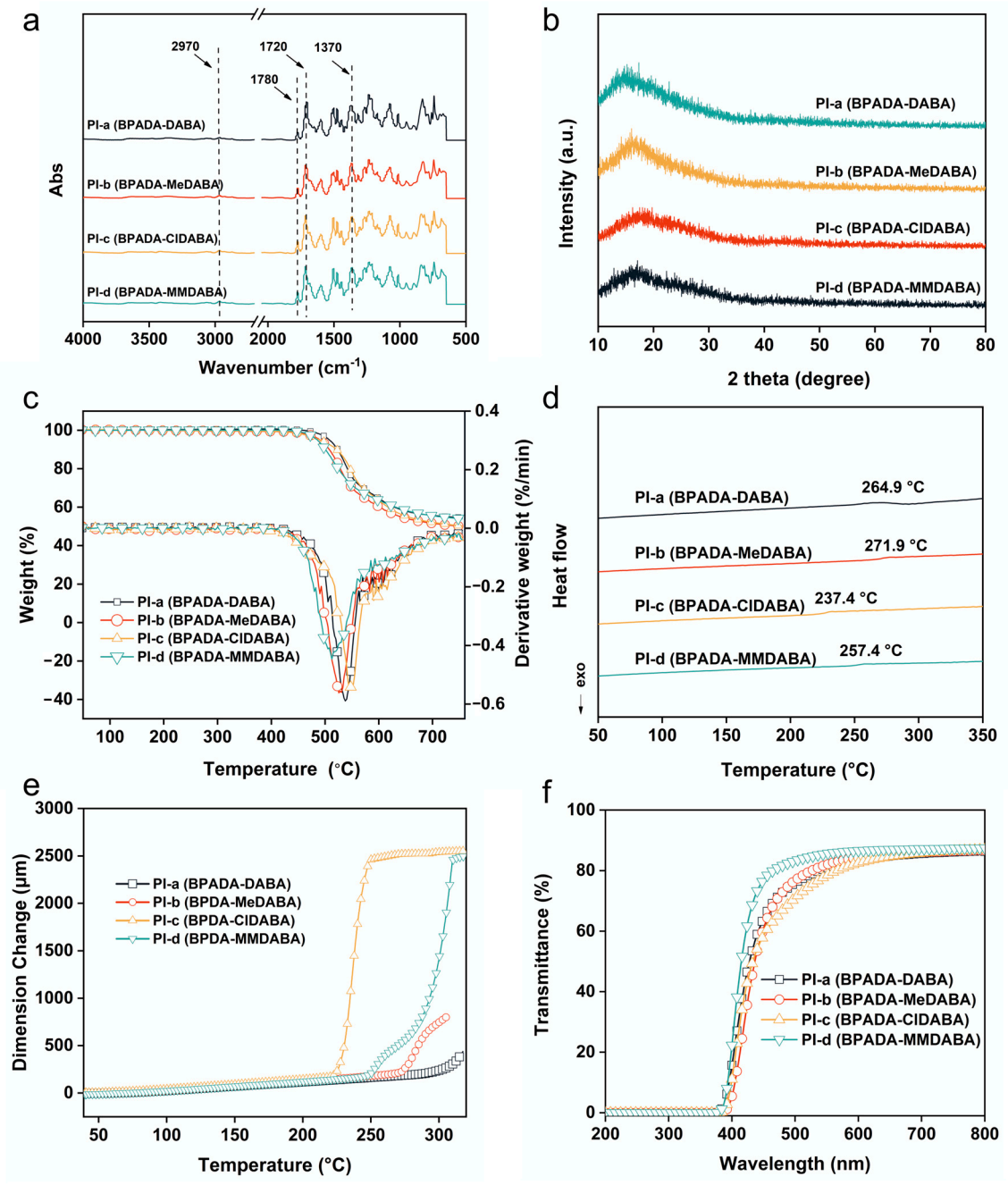

Figure 2. (**a**) FTIR spectra of PI films, (**b**) XRD spectra of PI films, (**c**) TGA and DTG curves of PI films in nitrogen, (**d**) DSC curves of the PI films, (**e**) TMA curves of the PI films, and (**f**) UV-Vis spectra of the PI films.

3.2. Thermal Properties

For the application of TENGs at high temperatures, it is imperative to select materials with exceptional thermal resistance. PIs, celebrated for their superior heat resistance, are highly advantageous for the development of TENGs intended to function under extreme conditions. The effects of amide functional groups on the high-temperature resistance of PI were investigated using TGA, DSC, and TMA tests, with the pertinent thermal data encapsulated in Table 2. A comprehensive mass change analysis of the PI films was conducted via the TGA technique over a temperature range from 50 °C to 750 °C, with the findings depicted in Figure 2c. As the temperature incrementally rises, a slow decrement in film mass was noted, with a slight weight loss of approximately 5% ($T_{5\%}$) being recorded

within the specific temperature range of 485 °C to 508 °C and the process being accelerated significantly within the narrow temperature range of 513–545 °C. Upon reaching 750 °C, the residual weight ratio (Rw_{750}) for the films ranged from 50.1% to 54.5%. Undoubtedly, the variation attests the remarkable thermal stability of the fabricated PI films and their capacity to retain structural integrity under elevated temperatures.

Table 2. Thermal properties of PI films.

Samples	$T_{5\%}$ [a] (°C)	T_{max} [a] (°C)	R_{w750} [a] (%)	$T_{g,\ DSC}$ [a] (°C)	$T_{g,\ TMA}$ [a] (°C)	CTE [a] ($\times 10^{-6}$/K)
PI-a	508	538	54.5	267	298	57.3
PI-b	491	526	50.1	272	280	63.7
PI-c	490	545	50.3	237	232	65.6
PI-d	485	513	54.1	257	249	61.2

[a] $T_{5\%}$: Temperatures at 5% weight loss; T_{max}: Temperatures at the rapidest thermal decomposition rate; R_{w750}: Residual weight ratio at 750 °C in nitrogen; $T_{g,\ DSC}$: Glass transition temperatures according to the DSC measurements; $T_{g,\ TMA}$: Glass transition temperatures according to the TMA measurements (peaks of tanδ plots); CTE: linear coefficient of thermal expansion in the range of 50–200 °C.

The thermal behavior of the PI films, specifically glass transition temperature (T_g), was meticulously assessed through DSC tests, with the results depicted in Figure 2d. The incorporation of flexible ether bonds generally lowers the T_g of the resulting PI, while the presence of the amide group and side methyl impedes the main chain's internal rotation, bolstering molecular chain rigidity and thus elevating the T_g values. Consequently, all PI materials maintain a T_g above 237 °C, demonstrating commendable high-temperature resistance. Moreover, the coefficient of thermal expansion (CTE) for this series of PI films was determined using TMA tests, with results depicted in Figure 2e. The findings indicate that all PI samples expand as the temperature rises, especially near respective T_g, where expansion becomes more significant. Due to the influence of more flexible chain segments, the CTE values for PI-a, PI-b, PI-c, and PI-d in the temperature range of 50–200 °C were found to be 57.3×10^{-6}/K, 63.7×10^{-6}/K, 65.6×10^{-6}/K, and 61.2×10^{-6}/K, respectively, demonstrating sufficient thermal stability for high-temperature applications.

3.3. Optical Properties

The specific impact of incorporating amide groups on the optical properties of the materials was examined through UV-Vis spectral analysis and CIE Lab color parameter measurements. Notably, research indicates that PI materials with optimal performance tend to exhibit higher transparency. Consequently, the molecular design and production methods for PI triboelectric materials align with those employed in developing colorless and highly transparent PI films. Thus, it is essential to examine the structure–property relationships of the newly developed PI films. The optical properties of the PI films, including the cutoff wavelength (λ_{cut}), the transmittances at the wavelengths of 400 nm (T_{400}) and 450 nm (T_{450}), the CIE color parameters of L*, a* and b*, and the haze, are detailed in Table 3. As shown in Figure 2f, the λ_{cut} of the PI films all surpassed 366 nm, with the T_{450} values of 64.1% for PI-a, 60.9% for PI-b, and 58.5% for PI-c, respectively. Notably, the T_{450} of the PI-d film attained 76.9%, demonstrating a significant enhancement in optical transmittance compared to the commercial Kapton® films. Moreover, to evaluate the optical properties in detail, the CIE Lab color parameters of the modified PI films were further measured. The results showed that the b* values of the PI films varied from 8.63 to 16.90 and the haze values from 0.52% to 1.16%, thus verifying the significant improvement in the optical properties. The incorporation of amide groups and associated side groups likely results in the stacking of the PI molecular chains in a more loosely packed arrangement. The arrangement increases the spatial separation between electron donors and acceptors, consequently reducing the charge transfer effect and contributing to the improved optical transparency of the material.

Table 3. Optical properties of the PI films.

Samples	λ_{cut} [a] (nm)	T_{400} [b] (%)	T_{450} [b] (%)	L* [c]	a* [c]	b* [c]	Haze (%)
PI-a	366	15.7	64.1	92.25	−2.37	12.83	1.00
PI-b	371	5.5	60.9	93.19	−4.25	16.90	0.52
PI-c	371	11.1	58.5	92.33	−1.54	12.85	0.68
PI-d	369	22.2	76.9	93.67	−2.52	8.63	1.16

[a] λ_{cut}: Cutoff wavelength; [b] T_{400}, T_{450}: Transmittance at the wavelength of 400 nm and 450 nm, respectively; [c] L*, a*, b*: color parameters.

3.4. Triboelectric Properties

The impact of amide group incorporation on output performance was evaluated through the engineering of a novel all-PI-based TENG, with the modified PI film serving as the positive friction layer and the FPI composite film as the negative friction layer. The performance of the specifically structured modified PI film within the TENG framework was thoroughly analyzed, with PA6 material also utilized in TENG devices for comparative purposes. Each TENG device underwent rigorous testing to measure its output under standardized conditions: a maximum contact pressure of 30 N, a working frequency of 2 Hz, and a spacer distance of 10 mm. The electrical outputs from these trials are detailed in Table 4. It is evident that TENG devices with distinct material combinations exhibit significant performance differences. As depicted in Figure 3a, the open-circuit voltage (V_{OC}) of the TENG with a PA6 tribo-positive material registered at 147 V. In contrast, the V_{OC} increased to approximately 169–181 V with PI-a to PI-c, and further elevated to about 242 V with PI-d as the positive friction layer. This trend persisted, as corroborated by the short-circuit current (I_{SC}) data in Figure 3b, where the TENG with PA6 generated merely 3.14 μA compared to the 5.62–8.13 μA output when implemented with the modified PI. These results unequivocally validate the superior triboelectric characteristics of molecularly modified PI films as a positive friction layer in TENG devices.

Table 4. Triboelectric properties of the TENG based on PI films.

Samples	V_{OC} (V) [a]	I_{SC} (μA) [b]	Q_{SC} (nc) [c]
PA6	147	3.14	46
PI-a	169	7.37	77
PI-b	181	5.62	80
PI-c	179	6.13	88
PI-d	242	8.13	117

[a] V_{OC}: open-circuit voltage; [b] I_{SC}: short-circuit current; [c] Q_{SC}: transferred charge.

In the transferred charge (Q_{SC}) test, the TENGs featuring the modified PI film demonstrated consistent performance in both voltage and current, as illustrated in Figure 3c. Notably, a TENG utilizing a PA6 material achieved a modest transferred charge of approximately 46 nC. In stark contrast, a TENG with a PI-d film as the positive friction layer attained a peak charge transfer of nearly 117 nC. This pronounced discrepancy underscores the pivotal role of modified PI materials in enhancing charge transfer efficiency. To further validate the superior performance of tribo-positive modified PI, the exceptional PI-d film was combined with conventional materials, including PA6 and commercial Kapton®. Various TENG devices were then constructed, and V_{OC} as compared under identical conditions, as shown in Figure 3d. The TENG made from PI-d/Kapton® material generated a positive voltage of 45 V, whereas the TENG built with PI-d/PA6 material yielded a negative voltage of 40 V. The outcome not only signifies the successful transition of PI from a traditionally tribo-negative materials to a tribo-positive materials, but also highlights its superior performance compared to the conventional PA6 material. These findings unequivocally affirm the exceptional triboelectric properties of the modified PI material, further cementing its advantages in triboelectric applications.

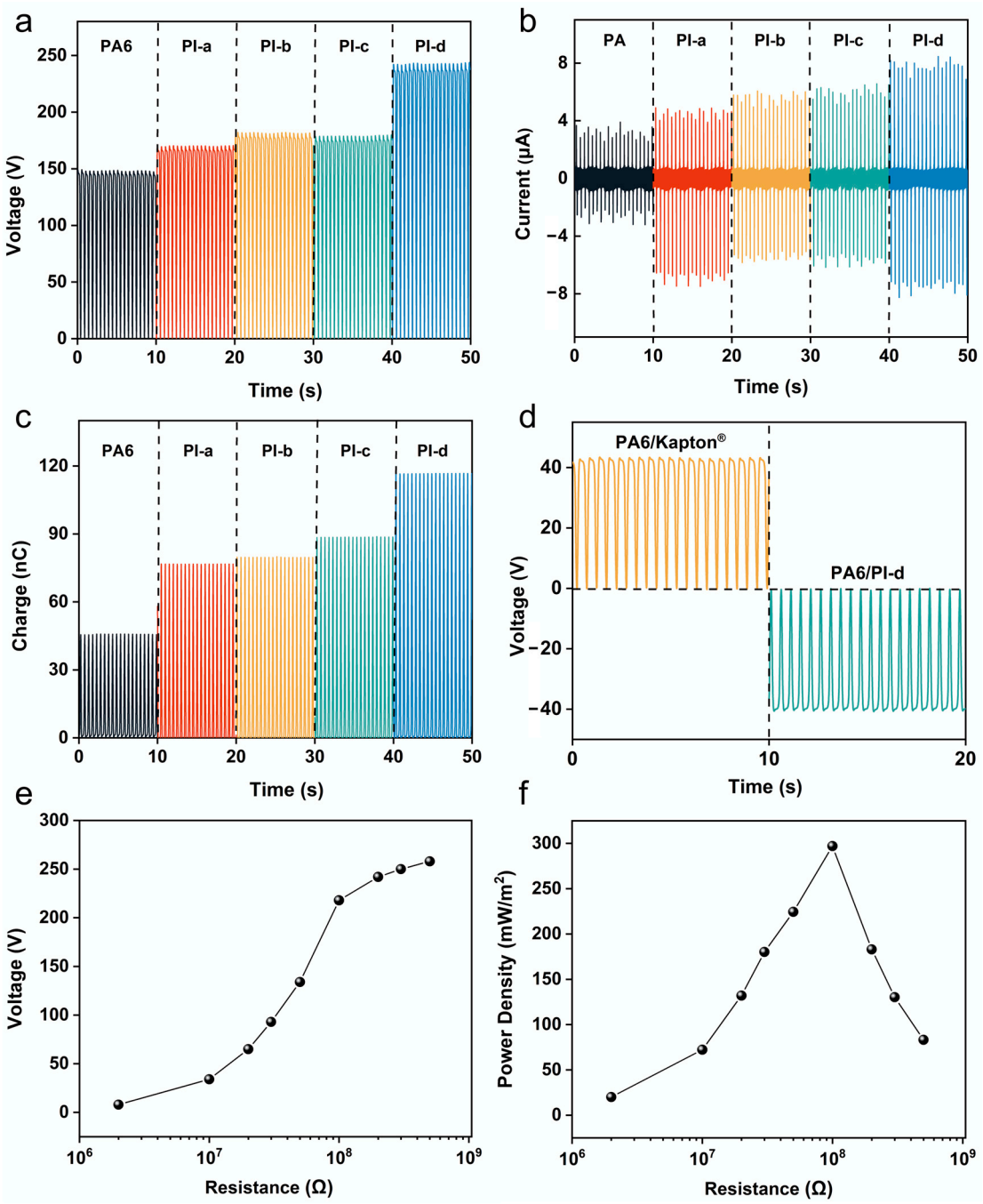

Figure 3. Output performance of the PI-based TENGs: (**a**) Open-circuit voltage, (**b**) Short-circuit current, (**c**) Transferred charge, (**d**) Open-circuit voltage comparison of different material combinations, (**e**) Output voltage under different loads, and (**f**) Instantaneous power density.

To meticulously assess the impact of load resistance on TENG's output, the systematic variations in load resistance were applied while monitoring changes in output voltage and power density. Figure 3e demonstrates that with a 2 MΩ external load, the peak output voltage reaches 8 V. With an increase in load resistance, the peak output voltage progressively rises, culminating in a significant surge to 258 V when the load resistance attains 500 MΩ. Conversely, as depicted in Figure 3f, the instantaneous power density initially increased with the increasing load resistance, eventually peaking before declining. At a load resistance of 100 MΩ, the TENG achieved a maximum instantaneous power density of 298 mW/m^2. These findings underscore that optimizing the load resistance can

significantly enhance the TENG's output power and expands its potential for a range of practical applications.

The extensive utility of modified PI as an exceptional tribo-positive material has been exemplified through the construction of TENGs, integrating PI films with various widely used tribo-negative materials, including PTFE, PDMS, and PVDF. A comprehensive evaluation of triboelectric properties was subsequently conducted, with the experimental findings presented in Figure 4. Comparative analysis revealed that TENGs with PI as the positive friction layer significantly outperformed those with PA6 in both V_{OC} and I_{SC}. These results underscore the superior performance of PI and confirm its remarkable adaptability and compatibility when paired with a diverse array of commonly used tribo-negative materials.

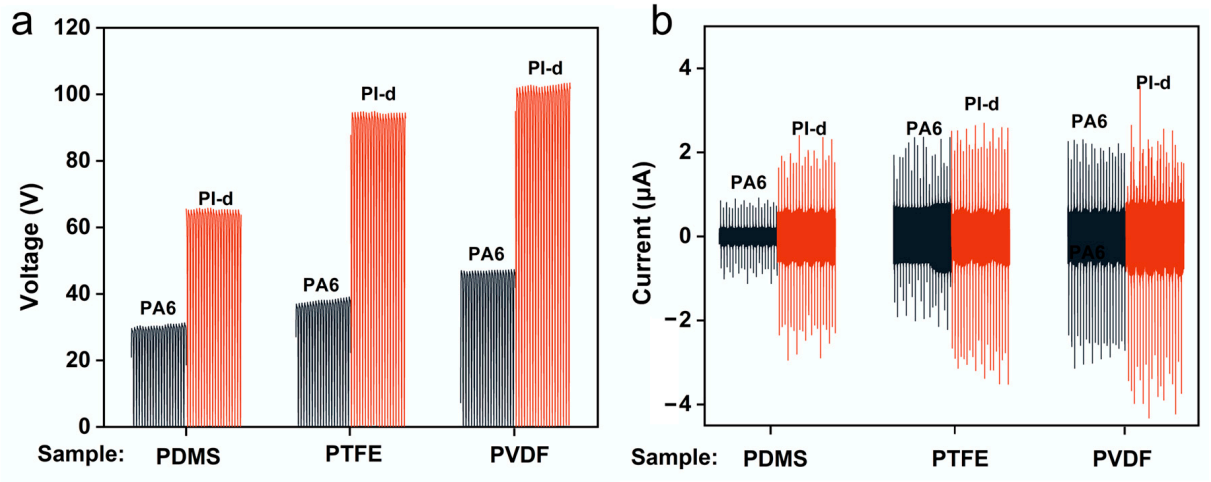

Figure 4. Output performance of TENGs assembled using various tribo-negative materials with PA6 and PI-d as the positive tribo-materials: (**a**) open-circuit voltage, (**b**) short-circuit current.

During the comprehensive evaluation of TENG performance, the I_{SC} response characteristics of modified PI films were systematically studied under variational contact force, working frequency, and spacer distance. Initially, the I_{SC} changes in the TENG device within the contact pressure range of 10 N to 40 N were recorded, with the working frequency set at 2 Hz and the spacer distance at 10 mm, as illustrated in Figure 5a,b. It was observed that the I_{SC} stabilized from 7.32 μA to 10.27 μA as the contact force increased from 10 N to 30 N, and peaking of 12.16 μA occurred at the contact pressure of 40 N, which indicates that increased contact pressure promotes the formation of additional microscopic contact points between the two materials, effectively enhancing the triboelectric effect by increasing the frictional contact area. Concurrently, the increase in contact pressure also induces the deformation of the material at the contact interface, further increasing the contact area. However, the increase in contact area will no longer be significant for the generation and accumulation of frictional charges as the plastic deformation of the material is close to or reaches its limit when the contact pressure reaches a certain threshold, leading to a saturation point in the improvement of performance. Additionally, the I_{SC} of the TENG was evaluated at a contact force of 30 N and a spacer distance of 10 mm, with varying working frequencies, as shown in Figure 5c,d. The data indicated that the I_{SC} significantly increased with the working frequency. The value of I_{SC} sharply rose from 7.43 μA to 11.42 μA when the frequency doubled from 1 Hz to 2 Hz. At a frequency of 4 Hz, the I_{SC} further escalated to 20.99 μA. The increase in working frequency is associated with an enhanced rate of charge transfer, which in turn increases the current output. As the frequency rises, the rate of material separation correspondingly increases, culminating in a more rapid charge transfer process. Consequently, a greater amount of charge traverses the circuit per unit time, resulting in a higher peak short-circuit current.

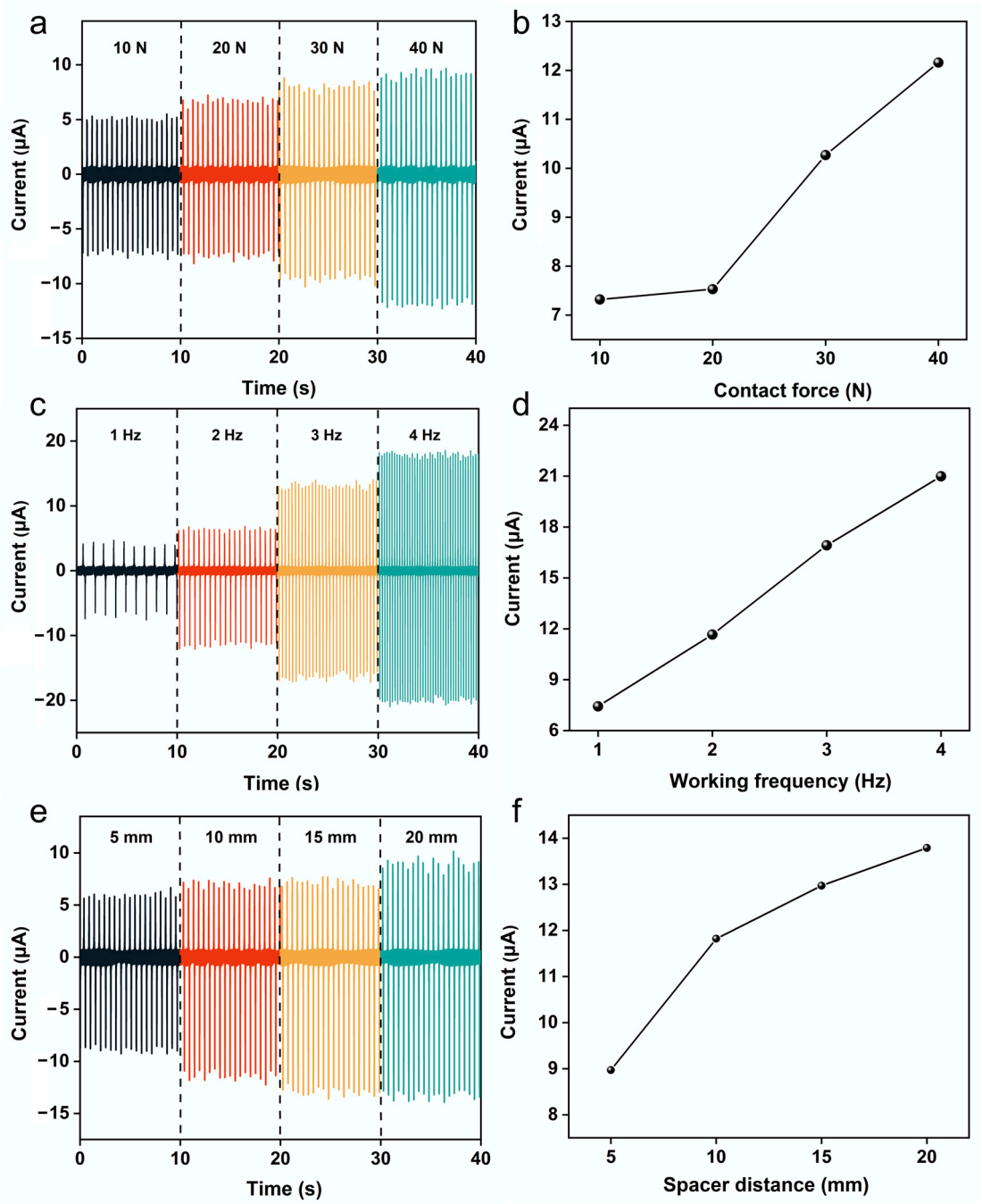

Figure 5. The short circuit current and variation trend (**a**,**b**) under a contact pressure range of 10 N–40 N, (**c**,**d**) under a working frequency range of 1 Hz–4 Hz, and (**e**,**f**) under a spacer distance range of 5 mm–20 mm.

The influence of the separation distance between the two triboelectric materials on the TENG's output performance was also examined. Under a constant contact force and working frequency, the I_{SC} was measured across a range from 5 mm to 20 mm, as depicted in Figure 5e,f. The I_{SC} exhibited a marked increase as the spacer distance grew from 5 mm to 15 mm, and it began to plateau beyond this distance. These findings indicate that at a steady operating frequency, an increase in spacer distance correlates with a higher velocity during the contact and separation of the triboelectric layers, thereby promoting electron flow in the external circuit and boosting the TENG's electrical output performance.

3.5. The Mechanism of Performance Enhancement

Polymers have emerged as essential materials for engineering high-performance TENGs due to their diverse functional group. The electron-donating or electron-withdrawing capabilities of these groups in polymers are predominantly influenced by inductive and conjugative effects. Amide groups, typically recognized as electron donors, play a pivotal role in the formation of tribo-positive materials. Within the PI structural system, the conjugation of an amide group with a benzene ring markedly amplifies its electron-donation potential, which in turn enhances the material's triboelectric characteristics. In this study, the triboelectric series of various polymer materials is presented, as delineated in Figure 6a.

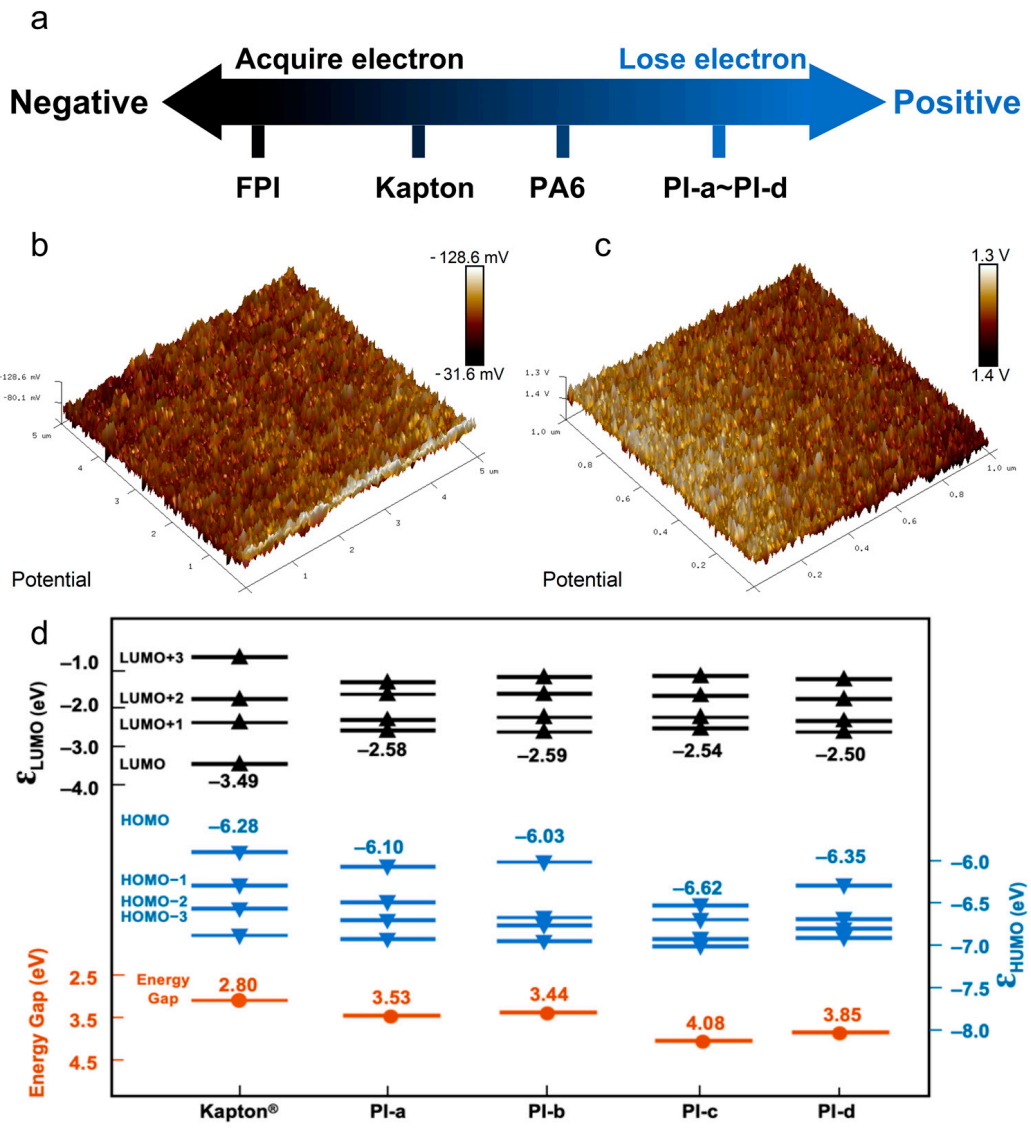

Figure 6. (**a**) Triboelectric series different polymer materials, (**b**,**c**) The KPFM measurement of 3D potential maps of PA6 and PI-d, (**d**) Energy level distribution diagram of the PI films.

The contact potential differences (CPD) were visualized to nullify as a voltage (V_{CPD}) applied between the tip and sample using Kelvin probe force microscopy (KPFM), which is crucial for evaluating charge transfer and retention [31]. As illustrated in Figure 6b,c, the PI-d film's CPD value was measured at 1.38 V, considerably surpassing the PA6 material's −0.07 V. This pronounced disparity underscores the PI-d film's enhanced positive triboelectric traits and its superior capacity to donate electrons during material interactions. Consequently, PI's efficacy in charge transfer, when utilized as a tribo-positive material,

facilitates a higher electrical energy output in TENG devices. The findings unequivocally demonstrate the exemplary performance of this series of PI films as positive triboelectric layers. To further elucidate the performance advantages of PI-based TENGs, the density functional theory (DFT) method was employed to calculate the orbital energy levels of PI molecules. The results, as presented in Figure 6d, highlight that the trend in the orbital energy levels upon the introduction of amide-based electron-donor groups is diametrically opposed to that observed with $–CF_3$ electron-withdrawing group [30,32]. Specifically, the HOMO energy level in the new PI series is significantly elevated, which is an advantage for the electron-donating capability. Furthermore, modifications in molecular structure yield energy gap (△ε, |εHOMO—εLUMO) values of 3.53 eV, 3.44 eV, 4.08 eV, and 3.85 eV, respectively, are considerably higher than the 2.80 eV band gap observed with Kapton®, allowing more localization for charge transfer to be maintained. Both experimental and theoretical investigations demonstrate that the molecular orbital of polymers play an important role in determining the triboelectric performance, thereby offering new possibilities for performance optimization in the design of tribo-positive materials for TENG applications.

3.6. Application Exploration

A durability test was conducted over an extended period to confirm the reliability of TENG devices fabricated with PI films. The linear motor cycle parameters were configured to standardize the frequency, force, and separation distance for each contact and separation event, ensuring repeatable test conditions. As depicted in Figure 7, the amplitude of the transferred charge exhibited no notable decline throughout the testing period during the continuous 1000 s cycles of contact and separation. The findings strongly suggest that the PI film-based TENG device demonstrates remarkable stability and long-term reliability.

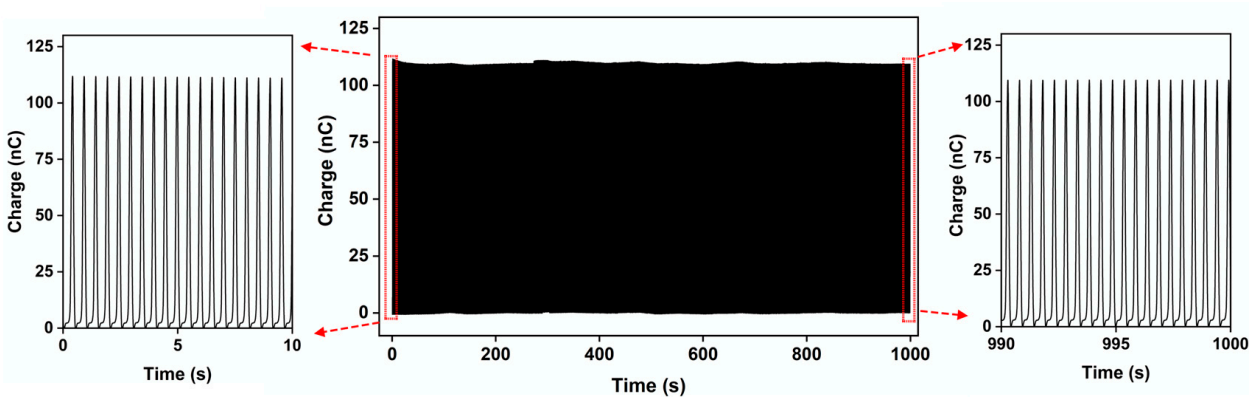

Figure 7. Transferred charge of TENG during 1000 s of continuous operation.

The operation of TENG is contingent upon the principles of electrostatic induction and the contact-separation mechanisms that occur between two distinct materials, thereby generating an alternating current. To fulfill the power needs for powering electronic devices, it is necessary to convert the alternating current output into the direct current output using a full-bridge rectifier circuit. Figure 8a illustrates the rectifier bridge circuit. The converted energy is then stored in capacitors or batteries, providing power to various external electronics. Under consistent experimental conditions, the TENG constructed from PI film was utilized to charge capacitors with varying capacities (1 μF, 3.3 μF, 4.7 μF, and 10 μF). The outcomes, displayed in Figure 8b, demonstrate that capacitors reached voltage levels of 10.2 V, 7.4 V, 5.8 V, and 3.4 V in 60 s, respectively. It was observed that the charging rate of the capacitors decreases with increasing capacitors. The phenomenon can be attributed to the limited quantity of charge produced by the TENG within a set timeframe, whereas larger capacitors require more charge to reach the same voltage level.

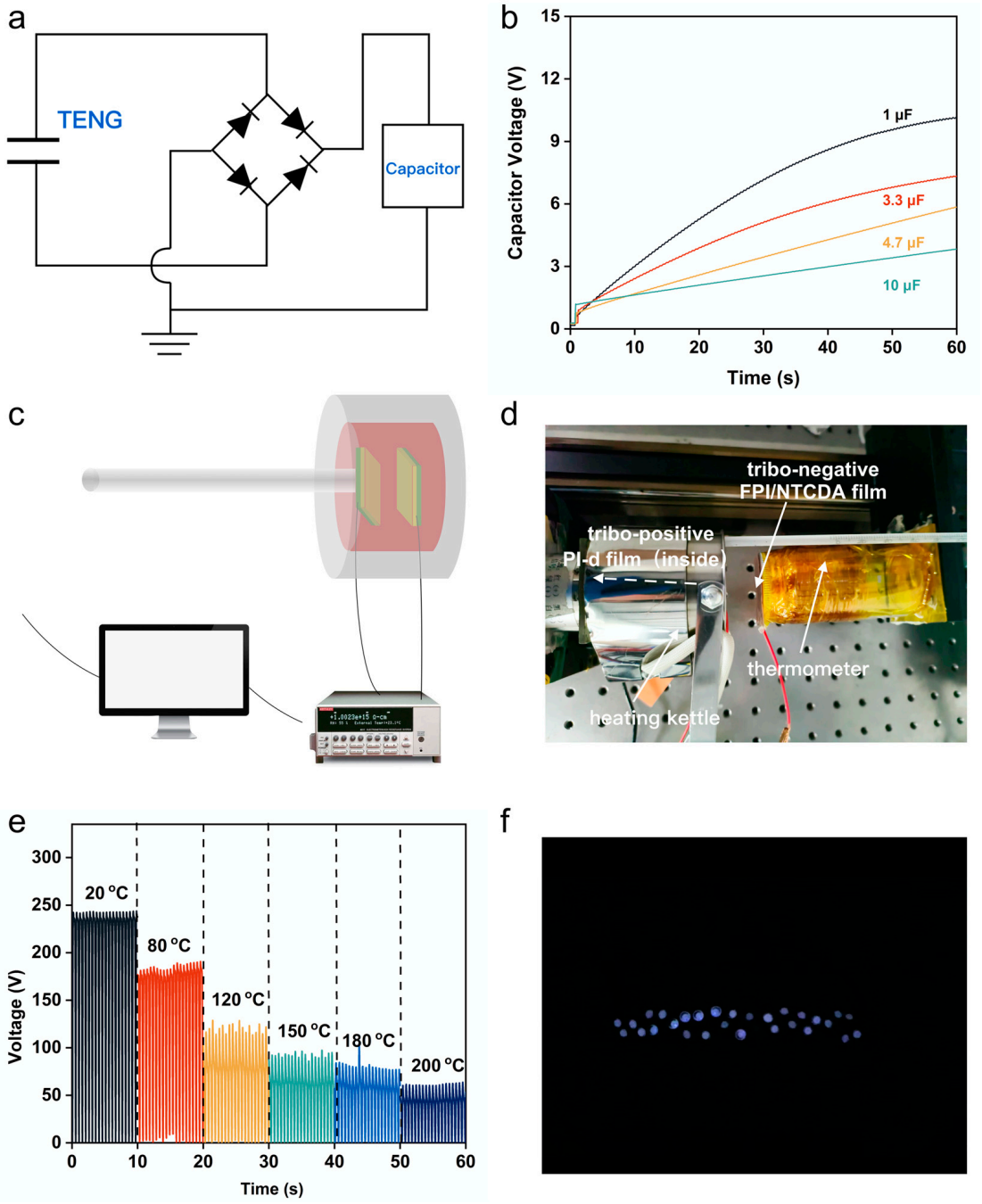

Figure 8. (**a**) Schematic of the TENG with rectifier circuit, (**b**) The capacitor voltage characteristics curves, (**c**) Schematic diagram of high temperature test setup, (**d**) Real picture, (**e**) Open circuit voltage of TENG at different temperatures, (**f**) The TENG lights up 30 LED bulbs at 200 °C environment.

To rigorously assess the robustness of the full PI-based TENG under high-temperature conditions, a test system comprising a heater, a linear motor, and an electrostatic meter was constructed. As depicted in Figure 8c,d, the impact of temperature fluctuations on the TENG's open-circuit voltage performance was evaluated. A decline in V_{OC} was observed as the testing environment's temperature increased, primarily attributable to the intensified thermionic emission effect, which facilitates charge escape from the PI material's surface. Nevertheless, the all-PI-based TENGs sustained a V_{OC} of 62 V even at extreme temperatures reaching 200 °C, as illustrated in Figure 8e. Furthermore, as evidenced by Figure 8f, a string of 30 series-connected LEDs consistently emitted light

at temperatures up to 200 °C during real-world application tests. These observations conclusively demonstrate the PI-TENG's capability to deliver a reliable electrical output, even under severe high-temperature conditions.

4. Conclusions

In this work, a novel tribo-positive PI material was synthesized by incorporating amide groups into the PI polymer backbone. This was achieved via molecular structural modifications, effectively altering the triboelectric characteristics of PI materials and the corresponding range of applications. The modified PI exhibited significantly superior tribo-positivity compared to traditional tribo-positive PA6 materials, attaining an open-circuit voltage of up to 242 V, a short-circuit current at 8.13 μA, and a transferred charge reaching 117 nC. Supporting evidence is provided by KPFM potential measurements, which reveal that the surface of PI exhibits more positive potentials compared to PA6. Additionally, DFT calculations suggest that the PI molecule possesses higher HOMO values and a larger band gap, corroborating the experimental findings. It is especially worth noting that these characteristics facilitate the PI-based TENG functionality at high temperatures, allowing for electricity generation and the illumination of a series of small LED bulbs at temperatures up to 200 °C.

Author Contributions: Conceptualization, J.L.; Methodology, S.Y., H.Y. and J.L.; Investigation, Z.P., Y.Z., X.R., Z.W. and Z.H.; Data curation, Z.P., Y.Z., X.R., Y.Q. and S.H.; Writing—original draft preparation, Z.P.; Writing—review and editing, J.L.; Supervision, S.Y., H.Y. and J.L.; Funding acquisition, S.Y. and J.L. All authors have read and agreed to the published version of the manuscript.

Funding: This work was supported by Shenzhen Science and Technology Program (No. JSGG20210629144539012).

Data Availability Statement: The original contributions presented in the study are included in the article, further inquiries can be directed to the corresponding author.

Conflicts of Interest: Author Shunqi Yuan was employed by the company RAYITEK Hi-Tech Film Company, Co., Ltd. The remaining authors declare that the research was conducted in the absence of any commercial or financial relationships that could be construed as a potential conflict of interest.

References

1. Fan, F.R.; Tian, Z.Q.; Wang, Z.L. Flexible triboelectric generator. *Nano Energy* **2012**, *1*, 328–334. [CrossRef]
2. Ren, Z.; Wu, L.; Pang, Y.; Zhang, W.; Yang, R. Strategies for effectively harvesting wind energy based on triboelectric nanogenerators. *Nano Energy* **2022**, *100*, 107522. [CrossRef]
3. Cheng, T.; Shao, J.; Wang, Z.L. Triboelectric nanogenerators. *Nat. Rev. Methods Primers* **2023**, *3*, 39. [CrossRef]
4. Yu, Y.; Gao, Q.; Zhang, X.; Zhao, D.; Xia, X.; Wang, J.; Wang, Z.L.; Cheng, T. Contact-sliding-separation mode triboelectric nanogenerator. *Energy Environ. Sci.* **2023**, *16*, 3932–3941. [CrossRef]
5. Jiang, D.; Lian, M.; Xu, M.; Sun, Q.; Xu, B.B.; Thabet, H.K.; El, S.M.; Ibrahim, M.M.; Huang, M.; Guo, Z. Advances in triboelectric nanogenerator technology-applications in self-powered sensors, internet of things, biomedicine, and blue energy. *Adv. Compos. Hybrid Mater.* **2023**, *6*, 57. [CrossRef]
6. Lu, P.; Guo, X.; Liao, X.; Liu, Y.; Cai, C.; Meng, X.; Wei, Z.; Du, L.; Shao, Y.; Nie, S.; et al. Advanced application of triboelectric nanogenerators in gas sensing. *Nano Energy* **2024**, *126*, 109672. [CrossRef]
7. Kumar, K.U.; Hajra, S.; Mohana, R.G.; Panda, S.; Umapathi, R.; Venkateswarlu, S.; Kim, H.J.; Mishra, Y.K.; Kumar, R.R. Revolutionizing waste-to-energy: Harnessing the power of triboelectric nanogenerators. *Adv. Compos. Hybrid Mater.* **2024**, *7*, 1–42. [CrossRef]
8. Wen, J.; Chen, B.; Tang, W.; Jiang, T.; Zhu, L.; Xu, L.; Chen, J.; Shao, J.; Han, K.; Ma, W.; et al. Harsh-environmental-resistant triboelectric nanogenerator and its applications in autodrive safety warning. *Adv. Energy Mater.* **2018**, *8*, 1801898. [CrossRef]
9. Cao, R.; Xia, Y.; Wang, J.; Jia, X.; Jia, C.; Zhu, S.; Zhang, W.; Gao, X.; Zhang, X. Suppressing thermal negative effect and maintaining high-temperature steady electrical performance of triboelectric nanogenerators by employing phase change material. *ACS Appl. Mater. Interfaces* **2021**, *13*, 41657–41668. [CrossRef]
10. Lai, J.; Ke, Y.; Cao, Z.; Xu, W.; Pan, J.; Dong, Y.; Zhou, Q.; Meng, G.; Pan, C.; Xia, F. Bimetallic strip based triboelectric nanogenerator for self-powered high temperature alarm system. *Nano Today* **2022**, *43*, 101437. [CrossRef]
11. Chen, Z.; Zhou, C.; Xia, W.; Yin, X.; Wang, Z.; Fu, X.; Liu, D.; Lv, J.; Liu, R.; Peng, Z.; et al. Strong, flexible and robust aramid nanofibers-based textile-triboelectric nanogenerators for high temperature escape monitoring and multifunctional applications. *Nano Energy* **2024**, *123*, 109359. [CrossRef]

12. Hu, J.; Qian, Y.; Wei, F.; Dai, J.; Li, D.; Zhang, G.; Wang, H.; Zhang, W. High powered output flexible aerogel triboelectric nanogenerator under ultrahigh temperature condition. *Nano Energy* **2024**, *121*, 109229. [CrossRef]
13. Kim, K.N.; Chun, J.; Kim, J.W.; Lee, K.Y.; Park, J.U.; Kim, S.W.; Wang, Z.L.; Baik, J.M. Highly stretchable 2D fabrics for wearable triboelectric nanogenerator under harsh environments. *ACS Nano* **2015**, *9*, 6394–6400. [CrossRef]
14. Shaukat, R.A.; Saqib, Q.M.; Kim, J.; Song, H.; Khan, M.U.; Chougale, M.Y.; Bae, J.; Choi, M.J. Ultra-robust tribo-and piezo-electric nanogenerator based on metal organic frameworks (MOF-5) with high environmental stability. *Nano Energy* **2022**, *96*, 107128. [CrossRef]
15. Han, G.H.; Lee, S.H.; Gao, J.; Shin, H.S.; Lee, J.W.; Choi, K.J.; Yang, Y.; Song, H.; Kim, Y.; Baik, J.M. Sustainable charged composites with amphiphobic surfaces for harsh environment–tolerant non-contact mode triboelectric nanogenerators. *Nano Energy* **2023**, *112*, 108428. [CrossRef]
16. Wang, F.; Wang, S.; Liu, Y.; Ouyang, S.; Sun, D.; Yang, X.; Li, J.; Wu, Z.; Qian, J.; Zhao, Z.; et al. Cellulose Nanofiber-Based Triboelectric Nanogenerators for Efficient Air Filtration in Harsh Environments. *Nano Lett.* **2024**, *13*, 4083. [CrossRef]
17. Qian, Z.; Li, R.; Guo, J.; Wang, Z.; Li, X.; Li, C.; Zhao, N.; Xu, J. Triboelectric nanogenerators made of polybenzazole aerogels as fire-resistant negative tribo-materials. *Nano Energy* **2019**, *64*, 103900. [CrossRef]
18. Lee, J.W.; Jung, S.; Jo, J.; Han, G.H.; Lee, D.M.; Oh, J.; Hwang, H.J.; Choi, D.; Kim, S.; Lee, J.H.; et al. Sustainable highly charged C_{60}-functionalized polyimide in a non-contact mode triboelectric nanogenerator. *Energy Environ. Sci.* **2021**, *14*, 1004–1015. [CrossRef]
19. Wu, J.; Wang, X.; He, J.; Li, Z.; Li, L. Synthesis of fluorinated polyimide towards a transparent triboelectric nanogenerator applied on screen surface. *J. Mater. Chem. A* **2021**, *9*, 6583–6590. [CrossRef]
20. Tang, N.; Zheng, Y.; Yuan, M.; Jin, K.; Haick, H. High-performance polyimide-based water-solid triboelectric nanogenerator for hydropower harvesting. *ACS Appl. Mater. Interfaces* **2021**, *13*, 32106–32114. [CrossRef]
21. Li, C.; Wang, P.; Zhang, D. Self-healable, stretchable triboelectric nanogenerators based on flexible polyimide for energy harvesting and self-powered sensors. *Nano Energy* **2023**, *109*, 108285. [CrossRef]
22. Ma, P.; Dai, C.; Wang, H.; Li, Z.; Liu, H.; Li, W.; Yang, C. A review on high temperature resistant polyimide films: Heterocyclic structures and nanocomposites. *Compos. Commun.* **2019**, *16*, 84–93. [CrossRef]
23. Liu, X.J.; Zheng, M.S.; Chen, G.; Dang, Z.M.; Zha, J.W. High-temperature polyimide dielectric materials for energy storage: Theory, design, preparation and properties. *Energy Environ. Sci.* **2022**, *15*, 56–81. [CrossRef]
24. Wan, B.; Zheng, M.S.; Yang, X.; Dong, X.; Li, Y.; Mai, Y.U.; Chen, G.; Zha, J.W. Recyclability and Self-Healing of Dynamic Cross-Linked Polyimide with Mechanical/Electrical Damage. *Energy Environ Mater* **2023**, *6*, e12427. [CrossRef]
25. Jia, T.; Fan, Z.; Zheng, S.; Zhou, H.; Chen, H.; Ma, N.; Liu, C. MWCNTs/polyimide multilayered aerogel-based paper enabling high-temperature-resistant and flexible sensor. *Chem. Eng. J.* **2024**, *492*, 152230. [CrossRef]
26. Yang, W.; Han, M.; Liu, F.; Wang, D.; Gao, Y.; Wang, G.; Xi, D.; Luo, S. Structure-foldable and performance-tailorable pi paper-based triboelectric nanogenerators processed and controlled by laser-induced graphene. *Adv. Sci.* **2024**, *11*, 2310017. [CrossRef]
27. Tao, X.; Li, S.; Shi, Y.; Wang, X.; Tian, J.; Liu, Z.; Yang, P.; Chen, X.; Wang, Z.L. Triboelectric polymer with high thermal charge stability for harvesting energy from 200 °C flowing air. *Adv. Funct. Mater.* **2021**, *31*, 2106082. [CrossRef]
28. Xing, F.; Ou, Z.; Gao, X.; Chen, B.; Wang, Z.L. Harvesting electrical energy from high temperature environment by aerogel nano-covered triboelectric yarns. *Adv. Funct. Mater.* **2022**, *32*, 2205275. [CrossRef]
29. Li, S.; Fan, Y.; Chen, H.; Nie, J.; Liang, Y.; Tao, X.; Zhang, J.; Chen, X.; Fu, E.; Wang, Z.L. Manipulating the triboelectric surface charge density of polymers by low-energy helium ion irradiation/implantation. *Energy Environ. Sci.* **2020**, *13*, 896–907. [CrossRef]
30. Pan, Z.; Yuan, S.; Ren, X.; He, Z.; Wang, Z.; Han, S.; Qi, Y.; Yu, H.; Liu, J. Preparation and characterization of fluorine-containing polyimide films with enhanced output performance for potential applications as negative friction layers for triboelectric nanogenerators. *Technologies* **2023**, *11*, 136. [CrossRef]
31. Ding, P.; Chen, J.; Farooq, U.; Zhao, P.; Soin, N.; Yu, L.; Jin, H.; Wang, X.; Dong, S.; Luo, J. Realizing the potential of polyethylene oxide as new positive tribo-material: Over 40 W/m^2 high power flat surface triboelectric nanogenerators. *Nano Energy* **2018**, *46*, 63–72. [CrossRef]
32. Lee, J.W.; Jung, S.; Lee, T.W.; Jo, J.; Chae, H.Y.; Choi, K.; Baik, J.M. High-output triboelectric nanogenerator based on dual inductive and resonance effects-controlled highly transparent polyimide for self-powered sensor network systems. *Adv. Energy Mater.* **2019**, *9*, 1901987. [CrossRef]